DOI: 10.13009/EUCASS2023-581
Aerospace Europe Conference 2023 – 10TH EUCASS – 9TH CEAS

Experimental validation of the electric sail concept

S. Mazouffre, U. Weller†*
** CNRS, ICARE laboratory, Orléans, France*
† CNES, French space agency, Propulsion, Pyrotechnie et Aerothermodynamie dpt, Toulouse, France
stephane.mazouffre@cnrs.fr – ulysse.weller@cnes.fr
*Corresponding Author

Abstract
The electric sail is a type of propellant-less propulsion system that relies on the solar wind dynamic pressure to create thrust and move a spacecraft. In this contribution, we present recent experimental results on ion deflection by an electric sail. The sail is here represented by a thin tungsten wire polarized to high positive or negative voltages. A low-power Hall thruster generates a quasi-neutral ion beam that mimics the solar wind. Various electrostatic probes are placed downstream of the sail to analyse the plasma disturbance created when the voltage is applied and ramped up. Ions are deflected whatever the applied voltage, the impact being more marked for large values. Experiments therefore indirectly demonstrate momentum from the beam is imparted to the wire, the core principle of an electric sail.

1. Introduction

The electric sail, or E-sail, is a type of propellant-less propulsion device for spacecraft that relies on the solar wind, a stream of charged particles released from the upper atmosphere of the Sun, called the corona, to generate thrust in contrast to the light sail that uses photons. The E-sail concept was proposed and developed by P. Janhunen in the 2000s as an efficient propulsion means for interplanetary and even interstellar journeys [1-3]. In short, an electric sail is a net of gigantic conducting wires, termed tethers, polarized to high voltages to disturb the trajectory of charged particles in such a way momentum from the solar wind is transferred to the structure, which generates thrust. An E-sail can operate either with a positive polarization, in that case ions are deflected and electrons are captured, or with a negative voltage, in that case electrons are attracted and ions are repelled. The first mode of operation is preferred as we shall see.
The left drawing in Figure 1 shows the architecture of an electric sail. Thin, (very) long and conducting wires are connected to a common point where the spacecraft and the payload are placed. They form the spokes of a wheel. The structure continuously rotates to maintain the spoke rigid and aligned thanks to the centrifugal force. Information about E-sail architecture, deployment and rotation strategies can be found elsewhere [4-12]. When the tethers are kept unpolarised, i.e. at the local floating potential, the size of the sail is extremely small as it simply corresponds to the geometrical area of all the tethers. In that case only a tiny fraction of the solar wind is captured and the net thrust is almost zero. In order to drastically improved the efficiency of an E-sail and the thrust level, tethers are polarized to a high voltage compared to the local plasma potential. As a consequence, the virtual area of the sail, i.e. the area seen by the charged particles of the solar wind, can be extremely large although the geometrical surface is extremely small, as illustrated in the right sketch of Figure 1. This originates from the fact that charged particles interact with the plasma sheath, a thick boundary layer that surrounds the wires. The latter increases with the voltage and varies as $n_e^{-0.5}$, where n_e is the plasma density. In the interplanetary medium, as the plasma density is very low, the plasma sheath can extend over 100s of meters with wires 100s of micrometers in diameter. The working principle of an electric sail is thus relatively straightforward and its architecture is simple and lightweight, making it attractive for exploration missions in deep space. The E-sail is nevertheless not without weak points. The main one is obviously the very low thrust level as the latter depends on the plasma density, the ion velocity and the tethers length and number. An electric sail is then a low-thrust low-acceleration propulsion means, which leads to very long trip duration [2]. Another drawback is the fact that the sail must constantly rotate, which requires energy. Finally, in order to maintain the quasi-neutrality of the local plasma, one must compensate for charged particle collection. In other words, charged particles have to be reinjected by the spacecraft into the plasma medium using particle guns. The latter require energy. Moreover, they decrease the E-sail reliability level and they may limit the device lifetime. The need of guns explains why a positive voltage is preferred for an electric sail. In that case electrons are captured and must be reintroduced using electron guns. This technology remains relatively simple compared with ion sources and it is nowadays well established and well mastered.

Copyright © 2023 by S. Mazouffre. Posted online by the EUCASS association with permission.

DOI: 10.13009/EUCASS2023-581

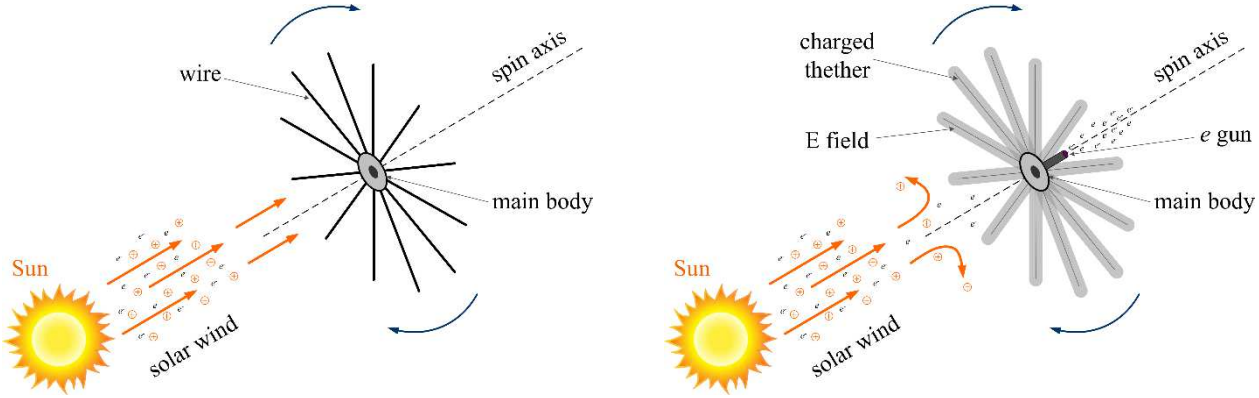

Figure 1: Sketch of an electric sail immersed in the solar wind. When the centrifugally stretched thin tethers remain floating the charged particle collection area is small and the net thrust is close to zero (left). When the tethers are polarized to a high positive voltage the effective sail area becomes much larger than the physical area of tethers and a relatively large thrust can be produced from the dynamic pressure of the solar wind (right). An E-sail includes an electron gun to return collected electrons to space, therefore quasi-neutrality of the local plasma, and maintain the positive bias of the tether assembly.

The thrust produced by an electric sail depends upon the local plasma density, the charged particle velocity, the tether geometrical characteristics and the applied voltage as shown in theoretical works by P. Janhunen and co-workers [2,4]. The solar wind mostly consists of electrons, protons and alpha particles with kinetic energy between 0.5 and 10 keV. At one astronomical unit (AU), the plasma density is around 7 cm^{-3}, which corresponds to a dynamic pressure of about 1 nPa. The low magnitude of the pressure explains the strong requirement on the E-sail dimensions, i.e. the tether length and number. According to the theoretical expression for the E-sail thrust, a tether polarized at 20 kV could produce a thrust of about 500 nN/m at 1 AU. It means that an E-sail composed of 10 tethers of 2 km in length could generate a thrust of 10 mN. The change of the thrust level with the distance to the Sun is exemplified in Figure 2 where the E-sail and the solar sail concepts are compared to one another. In the numerical simulations we considered a fully reflective 1000 m^2 solar sail and an electrical sail composed of 10 3 km long tethers polarized at +20 kV. As can be seen in Figure2, the solar sail thrust is larger close to the Sun, that means below ~2 AU. On the contrary, beyond 2 AU, the electric sail becomes more efficient in terms of thrust and the gap between the two technologies increases with the distance to the star. Theoretical calculations show that the thrust of an electric sail varies as $r^{-7/6}$, where r is the distance to the Sun, while is it proportional to r^{-2} for a solar sail. This is due to the fact that the force generated by an E-sail depends upon both the electron density and the Debye length. Figure 2 indicates the electric sail is an interesting low-acceleration spacecraft propulsion means for unmanned deep space missions towards far-off planets and even the edge of the solar system with relatively short trip time [13,14].

Although many theoretical and numerical works on electric sail have been performed over the past two decades, see e.g. references [2,4,15-18], only a very limited amount of studies were dedicated to the experimental verification of the E-sail concept either in the laboratory or in orbit, without success so far for demonstration in space. The ONERA team in France performed experiments in the JONAS vacuum chamber with a 5 mm in diameter metallic wire immersed in a low-energy (~ 30 eV) argon ion beam produced by a Kauffman-type gridded ion source [19]. They observed plasma disturbances around the wire due to a plasma sheath formation using electrostatic probes up to +1000 V. The team of Wiegmann and co-workers investigated the effect of a 1.85 mm in diameter stainless steel cylindrical tether polarized at +200 V on a 300 eV Ar^+ ion beam created with a Kaufman source [20]. They used a Differential Ion Flux Probe (DIFP) to get ion trajectory information [21]. Measurements show definitively the presence of a plasma sheath when there is a positive bias on the tether. They also indicate ions are deflected by the plasma sheath into large angle trajectories.
In this contribution, we present recent findings on sheath formation and ion deflection by a conducting wire polarized at high +/- voltages obtained in a vacuum chamber at low background pressure. A small low-power Hall thruster fed with krypton was used as a solar wind simulator. A 0.1 mm in diameter tungsten wire was vertically mounted downstream of the plasma source exit plane on the axis. A set of diagnostic was placed 5 cm behind the wire in the horizontal plane that contains the source axis. A Langmuir probe measured the electron parameters. A Faraday cup measured the ion current density. Finally, an energy analyzer recorded the ion kinetic energy. Measurements clearly reveal the impact of the polarization in both positive and negative modes upon the plasma flow. Ions are deflected

DOI: 10.13009/EUCASS2023-581

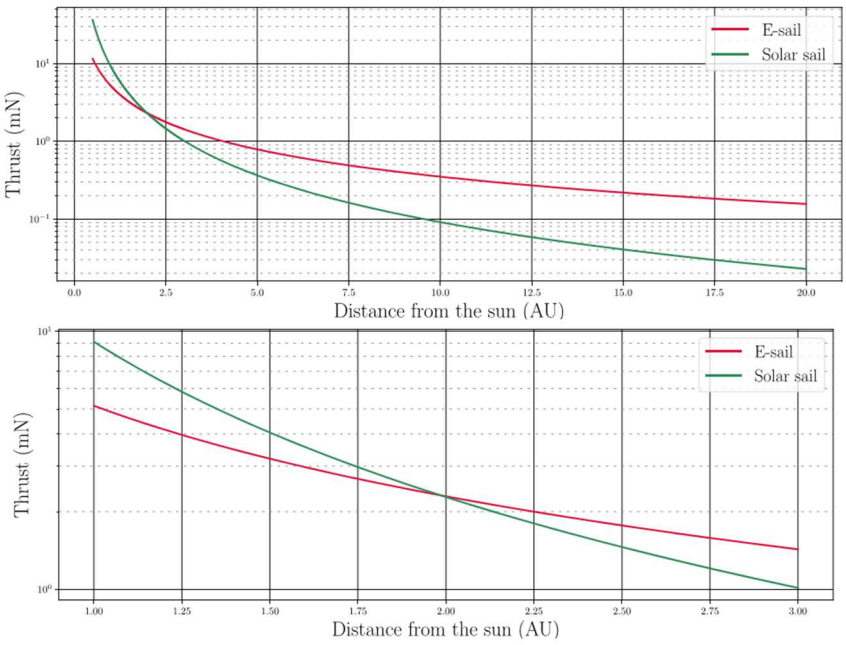

Figure 2: Numerical simulation of the thrust produced by a 1000 m^2 solar sail (green line) and a 10×3 km long tether assembly polarized at 20 kV as a function of the distance to the Sun (red line). The bottom plot shows the transition region between 1 and 3 AU. At large distances, the electric sail generates more thrust, that makes it an ideal propulsion means for rapid trips to either deep space or the inner solar system.

whatever the applied voltage, the impact being more marked for large values. Experiments indirectly demonstrate ions are deflected by a polarized tether, that means momentum from the charged particle beam is captured.

2. Experimental arrangement

Experiments were carried out in the NExET test bench of the ICARE laboratory. NExET is a non-magnetic stainless-steel vacuum chamber 1.8 m long and 0.8 m in diameter. Primary pumping is provided by a large dry pump that evacuates 80 m^3/h. A 1800 l/s in N_2 turbomolecular pump further pumps the chamber down to 10^{-6} mbar-N_2, by absorbing water vapor and light gases. The cryogenic pump absorbs gases such as xenon and krypton. The pumping speed is around 8000 l/s when the 0.5 m^2 cold panel is sustained at 35 K. The pump stack guarantees a residual background pressure around 10^{-4} mbar with krypton gas. The heavy particle momentum exchange mean free path is, in this backpressure condition, on the order of the chamber length, which guarantees a weak impact of the residual gas. A large water-cooled screen covered with graphite tiles is mounted at the back of the chamber. The screen absorbs a part of the ion beam energy, thereby reducing the thermal load on the cryogenic surface. The chamber is equipped with different observation windows, diagnostic ports as well as electrical, optical and gas feed-throughs. The interior of the test bench is easy to access using a large front door.

The 100 W-class ISCT100v2 Hall thruster was used as a plasma source in this study [22,23]. The ISCT100-v2 corresponds to the $2S_0$ configuration and it constitutes an example of a low-power Hall thruster. The annular discharge channel is made of BN-SiO_2. A non-magnetic stainless-steel ring anode is placed at the back of the discharge channel, against the internal surface of the outer ceramic wall. The propellant gas is injected homogeneously inside the channel through a mullite disk, of which the high porosity allows for diffusion of the gas. The magnetic field is generated by means of cylindrical samarium-cobalt permanent magnets, located on both sides of the annular channel. The symmetrical distribution as well as the lens-shape of the magnetic field are provided by a pure iron magnetic circuit. The maximum magnetic amplitude is reached at the channel exit plane, while a near-zero amplitude is reached in the anode area. A heated LaB_6 hollow cathode was used to generate the electron current needed for discharge balance and beam neutralization. The cathode was placed on top of the thruster slightly upstream the channel exit plane.

DOI: 10.13009/EUCASS2023-581

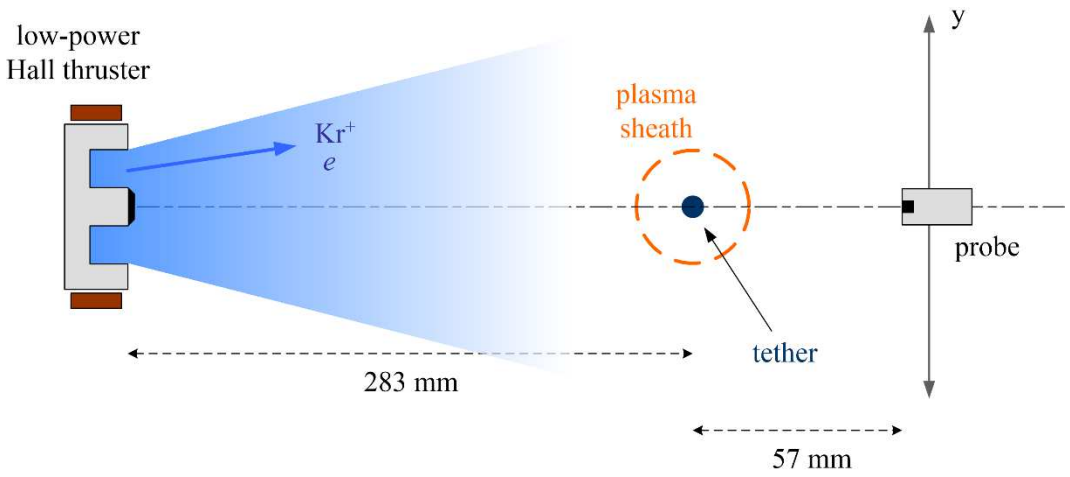

Figure 3: Layout of the experimental setup (not to scale). Electrostatic probes can move in the radial direction. The $y = 0$ position refers to the thruster centerline.

The Hall thruster was fueled with krypton (m = 83.8 amu) to generate a plasma jet. The gas mass flow rate injected into the channel was 7 sccm and the applied discharge voltage was set between 140 V and 170 V. With these parameters the source was stable and able to deliver [0.3 – 0.5] A of discharge current.

As previously explained, for an operational electric sail, the tethers are kilometers or even tens of kilometers in length. Obviously such tethers cannot fit inside vacuum chambers, therefore specific tether wire must be developed. In this study, a 64 mm long 0.1 mm in diameter tungsten wire was used as E-sail tether. Instead of applying a guarded design to minimize end effects, see [22,23], both ends of the wire were inserted into a small ceramic tube in such a way the exposed part is only 64 mm long. The wire was vertically mounted 28 cm downstream of the plasma source exit plane. The center of the wire was placed on the thruster axis to make the system symmetrical. A HEINZINGER PNC 20000 10 ump.60/721 Precision high-voltage power supply was used to bias the tether with positive or negative polarity. The device can provide a voltage up to 20 kV with a maximum current of 10 mA.

Three types of electrostatic probes have been employed to measure the plasma properties behind the wire. Probes were place 57 mm downstream of the wire as can be seen in Figure 3. The probe axis coincides with the thruster centerline. A linear translation stage allows to move the probe in the radial direction, i.e. perpendicular to the wire, over a ±50 mm distance. The largest view angle covered by probes is then 7.5°.

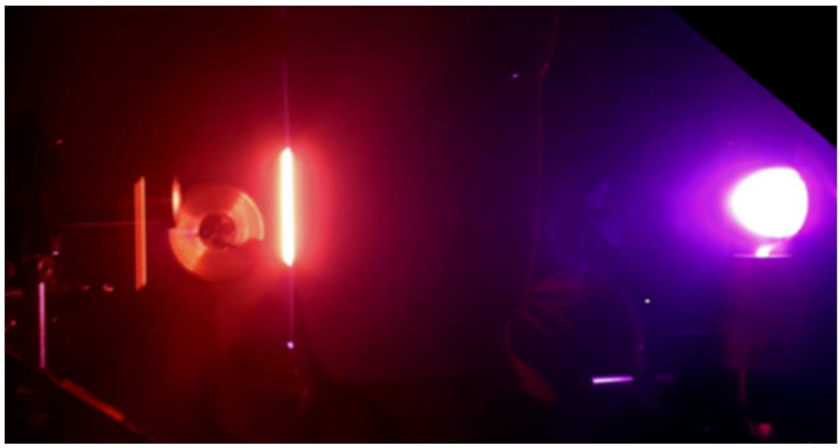

Figure 4: Photograph of the experimental setup during operation. The Hall thruster is located on the left. The tether is glowing red due to current collection. A Faraday cup is visible on the right.

DOI: 10.13009/EUCASS2023-581

A cylindrical Langmuir probe was used to determine electron properties from a I-V characteristic curve, see [24-26] and references herein. The probe active part is a 20 mm long and 0.4 mm in diameter tungsten wire. The cylindrical probe tip was aligned with the thruster axis. The local plasma potential V_p is derived from the I-V curve first derivative. The electron temperature T_e is computed from the slope of the ln(Ie) curve assuming a Maxwellian electron energy distribution function. Finally, the electron density $n_e \approx n_i$ is determined from the measured current in the ion saturation region using the Orbital Motion Limited theory.
A 40 mm in length Faraday cup with a 10 mm in diameter entrance collimator was used to determine the ion current density behind the tether [27,28]. The cup was polarized at -40 V to collect ions. The collimator was floating.
A compact Retarding Potential Analyzer (RPA), also known as Retarding Field Electrostatic Analyzer was used to determine the ion kinetic energy in the axial direction. In short a RPA is a gridded probe that uses electric fields acting as energy filters to selectively repel the constituents of a plasma or a beam [29-31]. The RPA used in this experiment is built with four electrostatically-biased grids and a collector placed behind the grids that serves as a charge detector. More information about the RPA design can be found in reference [22].

Figure 3 is a schematic of the experimental setup showing the main elements and their location. Note the y = 0 mm position refers to the plasma jet axis in the remainder of the article. Figure 4 is a photograph of the setup during operation and measurements. The active part of the wire is clearly visible as it is glowing red due to heating by the collected electron current.

3. Results and discussion

3.1 Tether I-V curve

The tether current-voltage characteristic curve is shown in Figure 5. The Hall thruster was operated at 145 V and delivered 0.3 A of current. The curve is a typical I-V curve of an electrostatic Langmuir probe. The electron current collected for positive bias is much larger than the ion current measured with negative voltages. Above 0.3 kV, the HV power supply saturated and the desired applied voltage could not be maintained. As can be seen in Figure 5, the ion current increases with the voltage that reveals the formation of a plasma sheath around the wire.

3.2 Electron properties

Figure 6 shows the electron temperature T_e measured in the radial direction for various values of the tether bias. The Hall thruster was fired at 140 V discharge voltage and I_d = 0.3 A. Probe data sets gathered downstream for a positively biased and a negatively biased tether are always compared to freestream data where there is no bias on the tether, i.e. the latter is floating. The floating tether case therefore correspond to the reference undisturbed case. Note that the wire has not been completely removed from the flow to determine the reference conditions. However, its presence has no impact as we shall see.

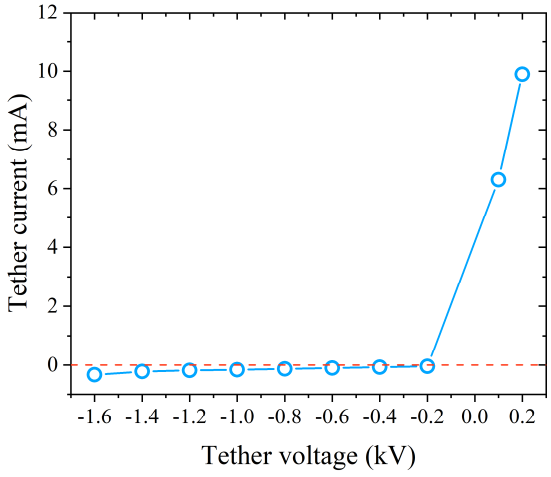

Figure 5: Current-voltage curve of the tether. The Hall thruster is fired at 145 V and 0.3 A.

DOI: 10.13009/EUCASS2023-581

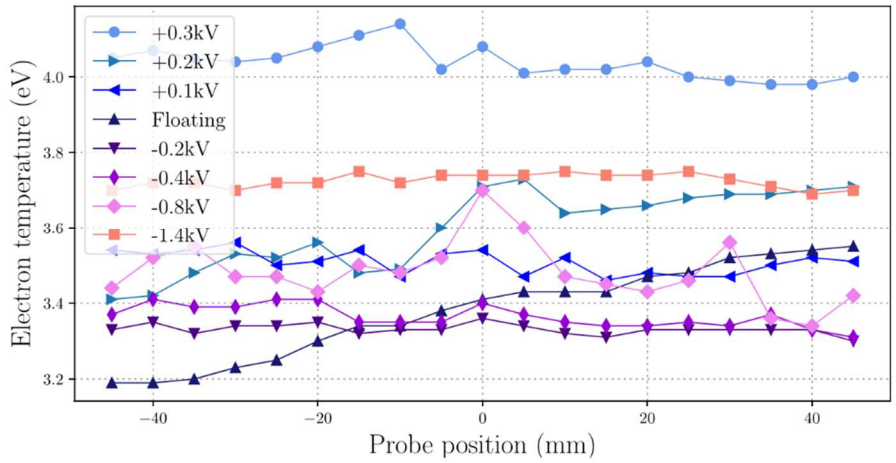

Figure 6: Electron temperature downstream of the tether as a function of the Langmuir probe position for various polarization voltages. The $y = 0$ position refers to the plasma jet axis.

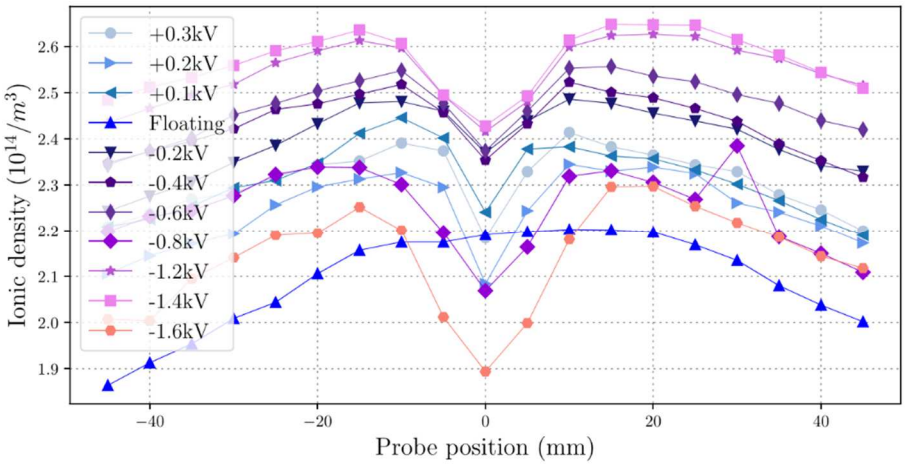

Figure 7: Electron density downstream of the tether as a function of the Langmuir probe position for various polarization voltages. The $y = 0$ position refers to the plasma jet axis.

Plots in Figure 6 indicate T_e is probably modified when the tether is polarized whatever the voltage magnitude and sign. An electron temperature around 3.5 eV in the far-field plasma plume region agrees with previous measurements carried out with a low-power Hall thruster [24,25]. The apparent offset may be due to a continuous drift in the chamber background pressure during measurement series. For LP series, the pressure increased from 7×10^{-5} mbar to 2×10^{-4} mbar owing to the heating of the cold surface of the bench cryo-pump during experiments.

The shift could also be a consequence of the tether bias. Measurements have been performed randomly in terms of wire voltage and taken over several days whereas Figure 5 shows a clear trend: the electron temperature increases when the tether voltage is ramped up for both positive and negative values. On the average T_e is around 3.4 eV for a floating wire. It gradually increases to about 4 eV at +0.3 kV and to about 3.7 eV at -1.4 kV. Such values indicate cold electrons are easier collected or deflected. The perturbation is apparently stronger for positive wire bias, that means when electrons are captured. The change in T_e seems to extend over a large area. One could have expected a perturbation more localized around the axis (y = 0 mm). The fraction of the beam that is probed is nevertheless relatively small as the view angle is 7.5°. Measurements over a broader region are then needed to clarify the influence of the tether voltage on the electron temperature.

DOI: 10.13009/EUCASS2023-581

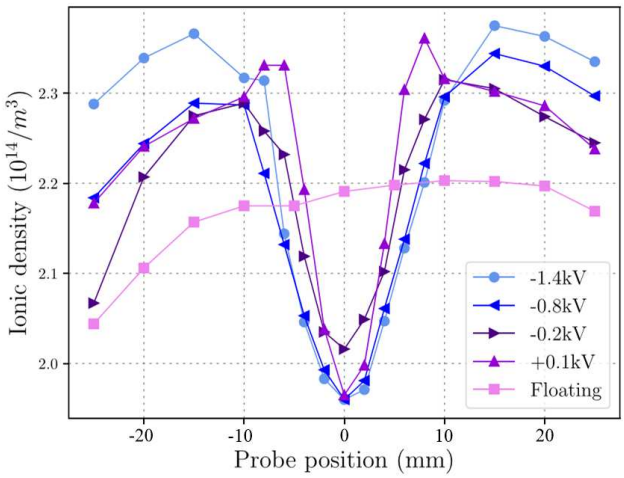

Figure 7: Second measurement series of ne profile downstream of the tether for various polarization voltages. A density overshoot is visible at the edges of the dip for positive voltages.

The radial profile of the electron density is given in Figure 7. The perturbation induced by the polarized wire is obvious. A dip appears in the electron density radial profile in the vicinity of the jet axis for negative and positive voltages. The dip size increases when the voltage magnitude is ramped up. This point will be further discussed in the next section. Comparisons between the floating and polarized tether cases show definitively the presence of a plasma sheath when there is a positive or negative bias on the tether. Experimental results demonstrate ions are deflected by the plasma sheath into large angle trajectories. They validate the principle of the electric sail.
In the probed region, the electron density increases when the wire is polarized as can be observed in Figure 7. The increase varies with the voltage, yet no clear trend can be noticed with our dataset. The entire probed region is disturbed when the tether is biased and the increase in n_e may be due to the scattering of charged particles at large angles. The zone surrounding the wire is depleted while the more distant areas are filled. Note that the density difference is around 0.5×10-14 m^{-3}, which is certainly within the error bar of our LP measurements.

A second series of measurements was taken to confirm the first experimental outcomes. The electron density distribution is given in Figure 8. A central void is present on the axis and the density in the wings increases when a voltage is applied to the wire. In addition, Figure 8 reveals an excess of charged particles in a narrow area at the edge of the void when the voltage is positive. This observation is in good agreement with PIC computer simulations [32].

3.2 Ion current

Figure 8 shows the radial distribution of the axial ion current measured with a Faraday cup. The Hall thruster was fired at 160 V discharge voltage and I_d = 0.3 A. The perturbation of the plasma flow due to the polarized tether is clear as a low flux region is created behind the tether for negative and positive voltages. Comparisons between the floating and polarized tether cases indicates ion trajectory is modified due to the formation of a plasma sheath around the wire. Note that the ion density decreases when the voltage amplitude is increased even far away from the axis, which means the induced perturbation expands. This trend is similar to the one observed with the plasma density, see Figure 7.

The width and the height of the dip in the ion current profile are presented in Figure 9 as a function of the voltage applied on the tether. The width here corresponds to the FWHM from the baseline. The wire is biased with a negative voltage and ions are collected. The solid red line represents a theoretical calculation of the high-voltage sheath thickness [33-37]. The calculation assumes a constant value of 65 µA for the ion current, i.e. the on-axis I_i value for the floating wire, and ion with 100 eV kinetic energy [37]. As can be seen in Figure 9, both the dip width and depth increase first and then start to saturate around ~1000 V. The width of the dip is of the same order of magnitude as the theoretical sheath thickness, i.e. around 1 cm. However, as the plasma sheath increases when the voltage is increased, the width of the ion current void reaches a constant value. This surprising experimental result is not yet understood, but two explanations can be proposed:

- Measurements are performed in a vacuum chamber that is relatively small and of which the metallic walls are grounded. The specific boundary conditions could limit the perturbation by acting as a charged-particle sink.

DOI: 10.13009/EUCASS2023-581

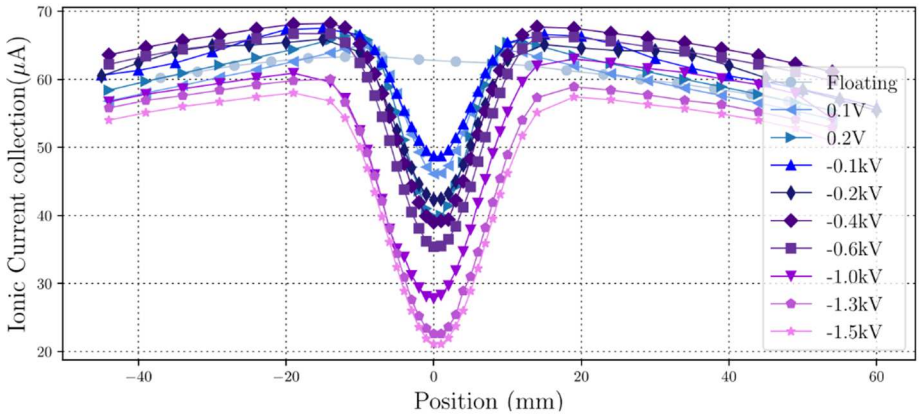

Figure 8: Axial ion current downstream of the tether as a function of the Faraday cup position for various polarization voltages. The $y = 0$ position refers to the plasma jet axis.

- The polarized wire is constantly bombarded by ions and the flux increases with the voltage magnitude, as shown in Figure 5. The ion current collection could lead to secondary electron emission. The latter counterbalance the electric field near the wire and prevent the sheath to expand [38-41]. At large voltages, the SSE should make the sheath vanish.

The first suggestion can be verified by carrying out experiments in a larger or a smaller vacuum chamber. The second idea can be tested by changing the wire material, as the SSE yield depends on the material nature, and by increasing the applied voltage (e.g. to reach the saturation regime where the sheath collapses).

Another interesting fact is illustrated in Figure 10. An excess in current is observed at the edges of the dip in the ion profile solely when the tether is positively biased. The current overshoot is not present with negative polarity. The small humps are also observed on the electron density radial profiles in Figure 7, however the effect is less clear as the spatial resolution was relatively poor. The experimentally found hump at the ion dip edges is in good agreement with particle-in-cell numerical simulations performed for a single 10 μm in diameter wire biased at +5.6 kV in the solar wind at 1 AU [32]. Figure 10 also shows the ion density given by the PIC simulations. The solar wind ions arrive from the left. Ions are clearly deflected by the charged wire and an empty wake is created behind the wire, which corresponds to the measured dip.

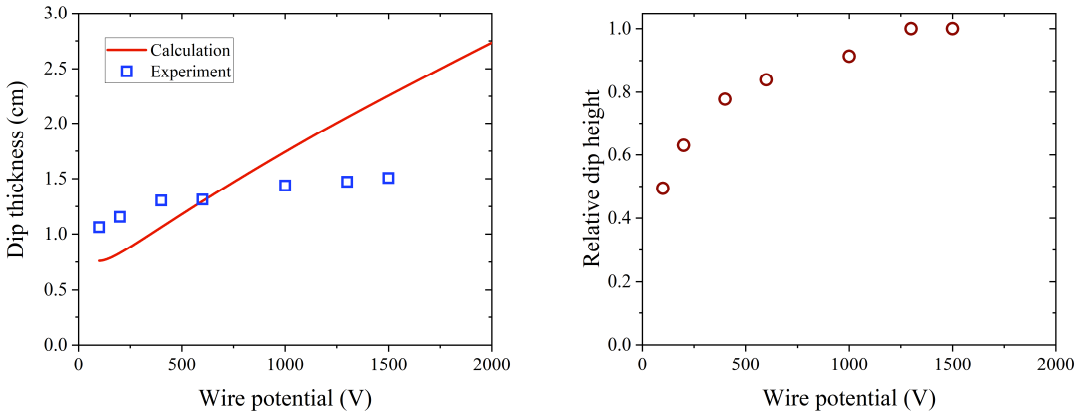

Figure 9: Left. Width of the dip in the ion current as a function of the voltage applied to the tether. The solid line is a theoretical calculation of the high-voltage plasma sheath around the wire. Right. Relative height of the dip in the ion current profile as a function of the tether voltage.

DOI: 10.13009/EUCASS2023-581

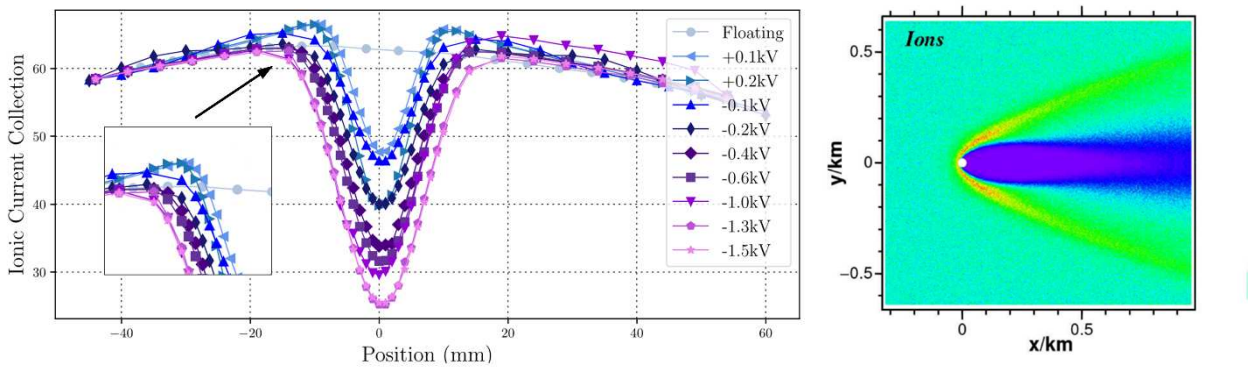

Figure 10: Hump at the edge of dip in the measured ion current profile for positive bias. Right. PIC simulation of the ion density for a wire at 1 AU biased at +5.6 kV [32].

3.3 Ion kinetic energy

As previously explained in the introductory section, a 4-grid RPA has been employed to measure the ion kinetic energy in the axial direction behind the wire. The Hall thruster was fired at 175 V with 0.5 A of discharge current to increase the RPA signal. The ion most probable energy is inferred from the first derivative of the RAP current-voltage curve. The MPE corresponds to the energy of the peak of the ion energy distribution function. The measured ion MPE is shown in Figure 11 for several tether voltages. At floating potential, the ion energy remains unchanged in the probed region in agreement with previous Hall thruster plasma plume measurements [22]: at small angle the energy does not vary. As can be seen in Figure 11, the tether voltage does not have a strong impact on the ion kinetic energy. Nevertheless, on average the ion energy seems lower when the wire is biased. Moreover, the energy decrease appears to increase when the voltage magnitude is increased. Results are consistent with a changed in the ion trajectories when the wire is polarized

One must keep in mind that here RPA measurements only provide the kinetic energy in the axial direction. As a consequence, we may capture a large fraction of ions that are neither repelled nor collected, i.e. ions with undisturbed trajectories.

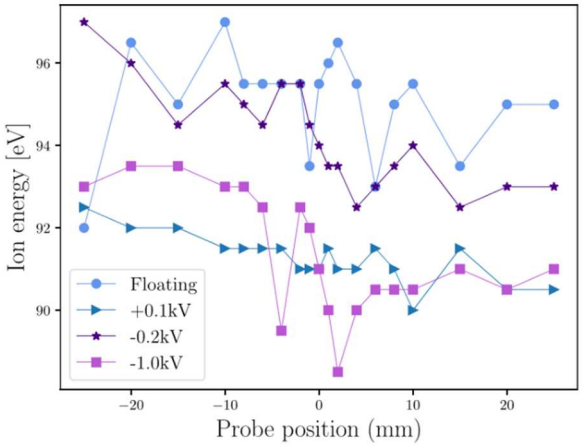

Figure 11: Ion most probable kinetic energy in the axial direction measured at several radial position for different voltages applied to the tether.

DOI: 10.13009/EUCASS2023-581

4. Conclusion

Experimental measurements carried out in a flowing krypton plasma produced by a low-power Hall thruster reveal the perturbation created by a polarized tether for both positive and negative voltages, in agreement with preceding numerical simulations. A polarized tether deflects ions and change their trajectories due to the formation of a plasma sheath around the wire. Momentum of the ion fluid is then transferred to the tether, which validates the operating principle of the electric sail. Some points nevertheless remain currently unexplained, namely the observed hump at the edges of the dip in the ion current distribution and the saturation of the dip characteristics, i.e. width and height, when the voltage increases.
Future works must first aim at clarifying those two points by performing measurements in a larger vacuum chamber, with lighter ions and with a gridded ion source that offers a more collimated plasma beam. A broader voltage range also has to be covered for the two polarities. Moreover, several tether materials should be used to examine the effect of the secondary electron emission yield. Finally, measuring the ion velocity vector would allow a better definition of ion trajectories and disturbances induced by a charged tether.

Acknowledgements

This work has been financially supported by the GAMA French startup (www.gamaspace.com).

References

[1] P. Janhunen, Electric sail for spacecraft propulsion, J. Propul. Power 20, 763-764 (2004).

[2] P. Janhunen, A. Sandroos, Simulation study of solar wind push on a charged wire: basis of solar wind electric sail propulsion, Ann. Geophys. 25, 755–767 (2007).

[3] M. Bassetto, L. Niccolai, A. A. Quarta, G. Mengali, A comprehensive review of electric solar wind sail concept and its applications, Progress in Aerospace Sciences 128, 100768 (2022).

[4] P. Janhunen et al. Electric solar wind sail: Toward test missions, Rev. Sci. Instrum. 81 111301 (2010)

[5] P Janhunen, A. A. Quarta, G. Mengali, Electric solar wind sail mass budget model, Geoscientific Instrumentation, Methods and Data Systems 2, pp. 85-95 (2013).

[6] P. Janhunen, P. Toivanen, TI tether rig for solving secular spinrate change problem of electric sail. arXiv Instrumentation and Method in Astrophysics, arXiv:1603.05563 (2016).

[7] P. Janhunen, P. Toivanen. An intrinsic way to control E-sail spin, arXiv Instrumentation and Method in Astrophysics, arXiv:1406.6847 (2014).

[8] P. Janhunen, Electric sail, photonic sail and deorbiting applications of the freely guided photonic blade, Acta Astronautica 93, pp. 410–417 (2014).

[9] P. Janhunen. Photonic spin control for solar wind electric sail, Acta Astronautica 83 pp. 85–90 (2013).

[10] J. Fulton, H. Schaub, Fixed-axis electric sail deployment dynamics analysis using hub-mounted momentum control, Acta Astronautica 144, pp. 160–170 (2018).

[11] J Fulton, H Schaub, Dynamics and control of the flexible electrostatic sail deployment, proceedings of the 26th AAS/AIAA Space Flight Mechanics Meeting, Napa, CA paper AAS 16-499 (2016).

[12] P. Toivanen, P. Janhunen, Electric solar wind sail: deployment, long term dynamics, and control hardware requirements, Advances in Solar Sailing, Springer, pp. 977–987 (2014).

[13] P. Janhunen, The electric sail - a new propulsion method which may enable fast missions to the outer solar system, J. British Interpl. Soc., 61, pp. 322-325 (2008).

[14] A. A. Quarta, G. Mengali, Electric sail mission analysis for outer solar system exploration, J. Guid. Contr. Dyn., 33, pp. 740-755 (2010).

[15] P. Janhunen, Increased electric sail thrust through removal of trapped shielding electrons by orbit chaotisation due to spacecraft body, Annales Geophysicae 27, pp. 3089–3100 (2009).

[16] P Janhunen. On the feasibility of a negative polarity electric sail, Annales Geophysicae. 27. pp. 1439–1447 (2009).

DOI: 10.13009/EUCASS2023-581

[17] P Janhunen et al., Using charged tether coulomb drag: E-sail and plasma brake, Proceedings of the 5th International Conference on Tethers in Space, Ann Arbor, Michigan, USA (2016).

[18] P. Janhunen, Simulation study of the plasma-brake effect, Annales Geophysicae 32, pp. 1207–1216 (2014).

[19] J.-M. Siguier et al, Drifting plasma collection by a positive biased tether wire in LEO-like plasma conditions: Current measurement and plasma diagnostic, IEEE Trans. Plasma Sci. 41 pp. 3380-3386 (2013).

[20] B. M. Wiegmann et al, The Heliopause Electrostatic Rapid Transit System (HERTS) - Design, Trades, and Analyses Performed in a Two Year NASA Investigation of Electric Sail Propulsion Systems, proceedings of the 53rd AIAA/SAE/ASEE Joint Propulsion Conference, Atlanta, GA, AIAA paper 2017-4712 (2017).

[21] N. H. Stone, Technique for measuring the differential ion flux vector, Rev. Sci. Instrum. 48, 1458, (1977).

[22] T. Hallouin, S. Mazouffre, Far-field plume characterization of a 100 W-class Hall thruster, AeroSpace 7, 58 (2020).

[23] S. Mazouffre, L. Grimaud, Characteristics and Performances of a 100 W Hall Thruster for Microspacecraft, IEEE Trans. Plasma Sci. 46, pp. 330-337 (2018).

[24] K. Dannenmayer, P. Kudrna, M. Tichý, S. Mazouffre, Measurement of plasma parameters in the far-field plume of a Hall effect thruster, Plasma Sources Sci. Technol. 20 065012 (2011).

[25] K. Dannenmayer, S. Mazouffre, P. Kudrna, M. Tichý, The time-varying electron energy distribution function in the plume of a Hall thruster, Plasma Sources Sci. Technol. 23, 065001 (2014).

[26] A. E. Vinci, S. Mazouffre, Plasma properties conditioned by the magnetic throat location in a helicon plasma device, J. Appl. Phys. 130, 183301 (2021).

[27] V. Hugonnaud, S. Mazouffre, Optimization of a Faraday cup collimator for electric propulsion device beam study: Case of a Hall thruster, Appl. Sciences 11, 2419 (2021).

[28] V. Hugonnaud, Plasma Probe Measurements for Electric Propulsion Device Ion Beam: Optimization and Standardization, PhD thesis, University of Vienna, Austria (2022).

[29] Gulbrandsen, A. Fredriksen, J. Carr, Jr., E. Scime, A comparison of ion beam measurements by retarding field energy analyzer and laser induced fluorescence in helicon plasma devices. Phys. Plasmas 22, pp. 1–15 (2015).

[30] D. Gahan, B. Dolinaj, M. B. Hopkins, Comparison of plasma parameters determined with a Langmuir probe and with a retarding field energy analyzer, Plasma Sources Sci. Technol. 17, 035026 (2008).

[31] C. Böhm, J. Perrin, Retarding-field analyzer for measurements of ion energy distributions and secondary electron emission coefficients in low-pressure radio frequency discharges. Rev. Sci. Instrum. 64, pp. 31–44 (1993).

[32] P. Janhunen, PIC simulation of Electric Sail with explicit trapped electron modelling, Proceedings of the 6th Intern. Conference of Numerical Modeling of Space Plasma Flows, Valencia, Spain, Vol. 17 pp. 271–276 (2011).

[33] B. Belinov, The Child–Langmuir law and analytical theory of collisionless to collision- dominated sheaths. Plasma Sources Sci. Technol. 18, 014005 (2009).

[34] K.-U. Riemann, The Bohm criterion and sheath formation. J. Phys. D: Appl. Phys. 24, pp. 492–518 (1991).

[35] P. Chabert, What is the size of a floating sheath? Plasma Sources Sci. Technol. 23, 065042 (2014).

[36] R. J. Umstattd, C. G. Carr, C. L. Frenzen, J. W. Luginsland, and Y. Y. Lau, A simple physical derivation of Child-Langmuir space-chargelimited emission usng vacuum capacitance. Am. J. Phys., 73, pp. 160–163 (2005).

[37] R. R. Puri, B. Debabrata, and R. Kumar, Generalization of the Child-Langmuir law for nonzero injection velocities in a planar diode. Physics of Plasmas 11, pp. 1178–1186 (2004).

[38] R. L. Petry, Critical potentials in secondary electron emission from Iron, Nickel and Molybdenum, Phys. Rev. 26, pp. 346 – 359 (1925).

[39] E.V. Alonso, M.A. Alurralde, R.A.Baragiola, Kinetic electron emission from solids induced by slow heavy ions, Surface Sci. 166, pp. 155–160 (1986).

[40] H. Eder, W. Messerschmidt, H. P. Winter, F. Aumayr, Electron emission from clean gold bombarded by slow Au^{q+} (q=1–3) ions, J. Appl. Phys. 87, pp. 8198–8200 (2000).

[41] C. Corbella, A. Marcak, T. de los Arcos, A. von Keudell, Revising secondary electron yields of ion-sputtered metal oxides, J. Phys. D: Appl. Phys. 49, 16LT01 (2016).